

**Deep Hubble Space Telescope<sup>1</sup>/Planetary Camera imaging  
of a young compact radio galaxy at  $z = 2.390$**

Rogier A. Windhorst

Department of Physics and Astronomy, Arizona State University,  
Box 871504, Tempe, AZ 85287-1504

William C. Keel

Department of Physics and Astronomy, University of Alabama,  
Box 870324, Tuscaloosa, AL 35487-0324

and

Sam M. Pascarella

State University of New York at Stony Brook  
Astronomy Program, Stony Brook, NY 11794-2100

Received \_\_\_\_\_; accepted \_\_\_\_\_

Send preprint requests to "raw@cosmos.la.asu.edu"

---

<sup>1</sup>Based on observations with the NASA/ESA *Hubble Space Telescope* obtained at the Space Telescope Science Institute, which is operated by AURA, Inc., under NASA Contract NAS 5-26555.

## ABSTRACT

We present deep 63-orbit *HST/PC* images at  $\sim 0''.06$  FWHM resolution in the filters  $B_{450}$ ,  $V_{606}$  &  $I_{814}$  — as well as in redshifted  $\text{Ly}\alpha$  — of the radio source LBDS 53W002, a compact narrow-line galaxy at  $z=2.390$ . These images allow us to distinguish several morphological components: (1) an unresolved nuclear point source ( $\lesssim 500$  pc at  $z=2.390$  for  $H_0 = 75$ ,  $q_0 = 0$ ), likely the central AGN which contains  $\lesssim 20\text{--}25\%$  of the total light in  $BVI$ ; (2) a compact continuum core ( $r_e \simeq 0''.05$ ); (3) a more extended envelope with an  $r^{1/4}$ -like light-profile and  $r_e \simeq 0''.25$  ( $\sim 2$  kpc); (4) two blue "clouds" roughly colinear across the nucleus aligned with the radio source axis and contained well within the size of the radio source.  $(B - I)$  color maps may suggest a narrow dust lane crossing between the nucleus and the smaller blue cloud. The radio source is *not* smaller than the distance between the blue continuum clouds, and coincides with a bright  $\text{Ly}\alpha$  "arc" in the western cloud, suggesting that jet-induced star-formation could cause both blue clouds, except the outer parts of the western cloud. The shape of this larger blue cloud suggests reflected AGN continuum-light shining through a cone (plus re-radiated  $\text{Ly}\alpha$  in emission). The OVRO interferometric CO-detection (Scoville et al. 1997) on *both* sides of 53W002 — and in the same direction as the continuum clouds *and* the radio jet — also suggest a star-bursting region induced by its radio jet, at least in the inner parts. Hence, both mechanisms likely play a role in the "alignment effect". Even at radio powers  $\sim 1.5$  dex fainter than the 3CR sources, we thus find many of the same aligned features and complex morphology, although at much smaller angular scales and lower optical-*UV* luminosities. We discuss the consequences for 53W002's formation in the context of the 16 sub-galactic objects at  $z \simeq 2.40$  around 53W002 (Pascarelle et al. 1996).

*Subject headings:* galaxies: evolution — galaxies: formation — galaxies:  
individual (53W002)

## 1. Introduction

To understand galaxy formation, one needs to observe high redshift galaxies at the highest possible resolution and sensitivity. This can be done with the  $0''.0455$  pixels of the Planetary Camera (*PC*) in the refurbished *HST* Wide Field Planetary Camera 2 (*WFPC2*), although sufficient surface brightness (SB) sensitivity can only be obtained with the *PC* for relatively compact objects. Jet-induced star formation or non-thermal radiation scattered in a reflection cone are the most probable radiation processes in ultraluminous high redshift 3CR and 1 Jy radio galaxies (Chambers, Miley & van Breugel 1990; McCarthy et al. 1991). It is not clear that these processes are universal, and their role needs to be clarified at high resolution for  $\sim 30\text{--}100\times$  weaker radio galaxies. To address these issues, we obtained deep multicolor high-resolution *HST/PC* images of the faint ( $V \simeq 23.0$  mag), compact ( $\lesssim 1''$ ), steep spectrum ( $\alpha \simeq 1.2$ ), radio ( $S_{1.4} \simeq 50$  mJy) galaxy LBDS 53W002 (Windhorst, van Heerde, & Katgert 1984a) which has *narrow* emission lines at  $z = 2.390$  (Windhorst et al. 1991; hereafter W91). 53W002’s radio power ( $\log P_{1.4} = 27.5 \text{ } W \text{ } Hz^{-1}$ ; using  $H_0 = 75 \text{ } km \text{ } s^{-1} \text{ } Mpc^{-1}$  and  $q_0 = 0.0$  throughout) is  $\sim 2.5$  dex above the FR-I/II break luminosity  $P^*$  at  $z=0$ . However, its compact radio morphology is *not* of FR-II type. Ground-based and pre-refurbished *HST continuum* images (Windhorst, Mathis, & Keel 1992, W92) showed some alignment with the radio source axis on  $0''.5\text{--}1''.0$  scales (4.5–9 kpc), which itself is aligned with the much larger ground-based  $Ly\alpha$  cloud ( $\sim 25 \times 45$  kpc; W91).

Our redshifted  $Ly\alpha$  images in the *WFPC2* medium-band filter F410M showed 16 possible compact  $Ly\alpha$  emitters surrounding 53W002 at  $z = 2.40$  (Pascarelle et al. 1996; P96). Nine of these objects have been spectroscopically confirmed thus far, possibly a group or cluster in formation (P96; Armus et al. 1997 in prep.; Keel et al. 1997, in prep.). The *PC* images were obtained to constrain the relative contributions from 53W002’s AGN and its young stellar population, and to examine the relations between these components

and its dynamics during the galaxy collapse — whether this occurred as a global halo collapse (*cf.* Eggen, Lynden-Bell, & Sandage 1962; ELS62), through the rapid merging of many sub-galactic sized objects (*e.g.*, Searle & Zinn 1978, SZ78; P96), through jet-induced star-formation (*e.g.*, Chambers et al. 1990), or a combination thereof.

## 2. *WFPC2* observations and processing

Deep *HST* exposures were taken with *WFPC2* in Cycle 4:  $12 \times 1700$  sec in the F606W (“V”,  $\lambda_{eff} \simeq 5940 \text{ \AA}$ ) and F814W (“I”,  $\lambda_{eff} \simeq 7920 \text{ \AA}$ ) filters. Two sets of  $6 \times 1700$  sec each were obtained at two different locations, taken a few days apart and separated by SAA passages (Driver et al. 1995a, D95a). In Cycle 5, four sets of  $6 \times 2400$  sec exposures were taken in F450W (“B”,  $\lambda_{eff} \simeq 4520 \text{ \AA}$ ; Odewahn et al. 1996; O96) and three sets of  $5 \times 2700$  sec exposures in the medium-band filter F410M ( $\lambda_{eff} \simeq 4090 \text{ \AA}$  or  $\text{Ly}\alpha$  at  $z \simeq 2.36 \pm 0.06$ ; P96). The 48-orbit stack of *BVI* images is shown as a color Plate in Fig. 1. The boxes show enlargements to the same angular scale for 53W002 and for the  $z = 2.40$  Objects 18 & 19 of P96 (seen in camera WF2). All calibrations and reductions followed Driver et al. (1995b), D95a, O96 & Windhorst et al. (1994a). A recent 10-hr 8.44 GHz VLA image with the C-array yielded three radio sources associated with the three AGN in Plate 1 with significant radio-optical offsets [ $\simeq (+0''.56, +1''.92) \pm 0''.14$ ]. This allowed us to bring the high resolution VLA 8.44 GHz (W91) and 15 GHz (Scoville et al. 1997; S97) images onto 53W002’s optical center — and likely its AGN (Fig. 2, §3.1) — to within  $\lesssim 3 \text{ PC}$  pixels.

## 3. Structure of the *PC* images of 53W002

Here we discuss the various discrete components of this young galaxy as revealed in the *PC* images. We emphase that given the fitting errors of the respective components,

and given the limit of the *HST/PC* resolution, the nature and quoted fluxes of each component (as fractions of the total flux) are not necessarily unique or uncorrelated, although the listed components are apparently necessary to make a full description of 53W002’s PC-morphology (see Fig. 2a–2f, Plate 2):

### 3.1. The maximum AGN contribution

To constrain the maximum possible AGN contribution to 53W002’s continuum, we subtracted a scaled PSF from the image core. As PSF, we used the faint red star ”S” noted by W92 (see Fig. 1 here) — circularly averaged to improve its S/N. The maximum possible point source that can be subtracted from 53W002’s core without making its central flux negative is  $25\pm2\%$  of the total light in *B*,  $21\pm3\%$  in *V*, and  $20\pm2\%$  in *I*. This light is contained within  $0''.06$  FWHM, or  $\sim 500$  pc, and has blue colors ( $B - I \simeq 0.06$  mag), as expected for an AGN at  $z \simeq 2.4$ . The upper error boundaries of these fractions are firm, so that the AGN contribution to 53W002’s total continuum is definitely  $\leq 30\%$ , but the lower boundaries are soft. The AGN contribution could be  $\lesssim 15\%$  of its total continuum, which would in Fig. 3 produce light-profiles that are straighter in  $r^{1/4}$ -space. These fractions are consistent with the spectroscopic limits (from C-IV/Ly $\alpha$  and N-V/Ly $\alpha$  ratios) to the AGN’s restframe UV-continuum fraction that is needed to power the high-ionization part of the Seyfert-like emission lines ( $\lesssim 35\pm 15\%$ ; W91), and with the  $30\pm 10\%$  value from the deconvolved Cycle 1 images (W92). 53W002’s AGN contribution is:  $V^{AGN} \simeq 24.3$ , or  $M_V^{AGN} \simeq -21.8$ , assuming a power-law *K*-correction with  $\alpha \simeq 1.0$  (W91, P96).

### 3.2. The inner resolved continuum ”core”

To address the symmetric extended component, we only consider and fit the “clean” quadrant between the blue clouds discussed in §3.4 (Fig. 2a–2f). The central parts of the galaxy in F450W cannot be simultaneously fit by a single  $r^{1/4}$  or exponential law. Comparing these profile-fits to the PSF shows that a small additional central light distribution (with  $r_e \sim 0''.05$ ) is required, containing about half the flux of the nuclear point source, but with redder colors ( $B - I = 0.8 \pm 0.1$ ).

### 3.3. The remaining $r^{1/4}$ -like profile

After subtraction of the central unresolved AGN component (§3.1), the underlying galaxy can be measured only in the quadrant *between* the two blue clouds (§3.4). We concentrate on a region south of the nucleus, where nearly a full  $90^\circ$  quadrant is clear of these contaminating sources. Details of the elliptical profile fitting technique and its errors are given by W92, Keel & Windhorst (1993), Windhorst et al. (1994b, W94b), Mutz et al. (1997; M97), and Schmidtke et al. (1997; Sc97). The major source of error is the sky-subtraction, but the sky in the PC-image stack is sufficiently low and flat that sky-subtraction errors are  $\lesssim$  few % of sky. Given these caveats, the  $BVI$  light-profiles (Fig. 3) follow an  $r^{1/4}$ -like profile closer than an exponential disk, although an early-type galaxy with a bulge-to-disk ratio  $\gtrsim 3$ –5 cannot be ruled out. Most of the deviation from an  $r^{1/4}$ -law at  $r^{1/4} \gtrsim 0.75$  ( $r \gtrsim 0''.32$ ) occurs in  $B$  &  $V$ , and is due to the faint blue cloud leaking into the uncontaminated quadrant, and not only due to sky-subtraction errors, which affect the profile for  $SB_{BVI} \gtrsim 25.5$ –26.0 mag arcsec $^{-2}$ . We fit a family of  $r^{1/4}$ -profiles — convolved with the PSF (§3.1) — to the  $PC$  data in this area over the radial range  $r=2$ –9 pixels ( $0''.1$ – $0''.4$ ). The best  $r^{1/4}$ -fit has (a/b)= $1.25 \pm 0.1$  and  $r_e \simeq 0''.20 \pm 0.07$  in  $B$  &  $V$ , and  $r_e \simeq 0.27 \pm 0.05$  in  $I$  (or 1.8–2.5 kpc), pointing at best to a small color gradient. Its position angle ( $PA \sim 110^\circ$

) is uncertain, but consistent with the orientation of the aligned clouds ( $PA \sim 95^\circ$ ), which appear to be separated by a redder feature (§3.4 & Fig. 2f). The  $I$ -band profile is dominated by the continuum — and least affected by the blue clouds which contribute  $\sim 8\%$  of the total  $I$ -band flux — and is a somewhat better  $r^{1/4}$ -fit, consistent with a crossing time of collapsing galaxies that increases with radius (Fig. 1g in van Albada 1982).

53W002’s average color is  $(B - I) \simeq 1.3$ . Its  $(V - I)$  color of  $\sim 0.7$  is less contaminated by the blue cloud. Within the errors, both colors are relatively constant with radius, so that any color gradient must be small for  $r \lesssim 1''0$  ( $\lesssim 0.3$  mag across the  $PC$  image). W91 & W94b present 12-band ( $Ly\alpha$   $UBVRIGriJHK$ ) photometry for 53W002 and surrounding objects, and W94b, M97, & Sc97 discuss spectral evolution model fits to these, and similar, color-redshift data to constrain stellar population ages (defined as the onset of the major visible starburst). The general blue colors in Fig. 2f suggests that, with the exception of the region possibly affected by a ”dust lane”, 53W002 is not enormously reddened by dust (§3.4). Following these models, the colors of the symmetric component of 53W002 — if interpreted as coming from stars only — would suggest a stellar population with an average age of  $\sim 0.4$  Gyr, which is of the same order as its dynamical time scale (§4). Without the detection of a significant color gradient in the stellar population, the current data cannot distinguish whether 53W002 formed through a sudden, global halo collapse (*cf.* ELS62) or through rapid merging of many sub-galactic sized units (*e.g.*, SZ78, P96). *HST/NICMOS*  $J, H$  images that bracket the  $4000\text{\AA}$  break will help decide between these scenarios. Below we show that there may be other processes triggering the (star)formation of 53W002.

### 3.4. The nature of the blue clouds

The residuals after removing the symmetric pieces described in §3.1–3.3 trace the aligned blue ”clouds” nicely. The larger cloud to the west — in the direction of the

extended Ly $\alpha$  cloud (Fig. 2a & W91) — is quite extended and vaguely triangular (Fig. 2e and insert in Fig. 1). It peaks 0".45 west of the nucleus and extends  $\gtrsim 1''$  from the core with an opening angle of about  $45^\circ$  (Fig. 2b). In Ly $\alpha$ , it is dominated by a brighter "arc" about 0".6 from the core (Fig. 2a). On the opposite side is a very small blue object — possibly a "counter-cloud" — elongated perpendicular to the nucleus-cloud direction and confined within 0".2 from the core (Fig. 2e) — at the very limit of the *HST/PC* resolution. These blue "clouds" comprise 13% and 5%, respectively, of the total F450W flux, and probably account for a good fraction of both the size [ $r_e$  (I)  $\sim 1''.1$ ] and elongation of 53W002 inferred from the pre-refurbished WFC images in *V* & *I* (W92). Hence, we now interpret 53W002's stellar light distribution as much smaller and less elongated. Similar analysis of the PC-images in  $V_{606}$  &  $I_{814}$  (with correspondingly reduced angular resolution) shows the same basic components (Fig. 2c & 2d). The core and small extended region immediately surrounding it are significantly bluer than their surroundings, as is the western extended cloud (Fig. 2f). With the exception of the "arc" at the edge of the larger cloud, the aligned components and the core are essentially free of Ly $\alpha$  line-contamination (Figs. 2a–2f). The nucleus is a weak Ly $\alpha$  source, contributing only about 20% of the total Ly $\alpha$  flux (Fig. 2a). Ly $\alpha$  contributes about 17% of the overall *B* light in a 2".5 aperture, somewhat smaller than the  $\sim 30\%$  expected from the integrated spectrum (W91 & P96). That is, the Ly $\alpha$  line emission is no more concentrated than the continuum light, and is thus not dominated by the nucleus. In the eastern cloud, Ly $\alpha$  contributes no more than 10% of the *B*-band flux, but the "arc" at the outer edge of the western cloud contributes as much as 93%. This is the only feature seen in the Ly $\alpha$  image with significant contrast against the rest of the galaxy in terms of equivalent width. These two blue clouds could represent:

- (1) Reflection of the AGN-light shining through a cone, including Ly $\alpha$  and C-IV emission lines from gas lit up by the cone. The asymmetry in size and flux between eastern and western clouds (Fig. 2b & 2e) may represent obscuration or genuine physical

differences. The fact that we can see a much larger and somewhat symmetric ground-based Ly $\alpha$  cloud (compare our Fig. 2a to Fig. 3 of W91) argues against obscuration, although this extended Ly $\alpha$  gas could be mostly in front of — or away from — any dust, and in part be unrelated to the AGN. We note that two other  $z \simeq 2.40$  objects (Obj. 18 & 19 of P96) are also AGN with continuum reflection cones (see inserts in Plate 1), but with a relatively stronger AGN component compared to the surrounding material (at the 50–80% level of the total flux). The presence of these reflection cones implies the existence of a substantial amount of gas and/or dust well beyond the optical extent of these galaxies (see §4).

(2) A star-bursting region induced by 53W002’s radio jet. Compared to the spectral evolution models described by W94b, the much bluer colors of the cloud — if caused by stars — would suggest a star-bursting region  $\lesssim 10^8$  years old. This is similar to the typical radio source lifetime, but younger than the galaxy’s dynamical time scale.

A color map — produced by matching the registration, sampling and resolution of the  $B_{450}$  &  $I_{814}$  images — shows the color contrast between the inner and outer regions of 53W002 (Fig. 2f). This map also provides an interesting clue as to the possible origin of the smaller “cloud” seen near the nucleus in the  $B_{450}$  images: a red, almost linear feature appears to separate this smaller cloud from the nucleus. In nearby galaxies, this would suggest an organized dust lane. The color of the outskirts of this smaller cloud is  $(B - I) \simeq 0.6$  (at  $r=0''.13$ ), and for the red “dust” lane it is  $(B - I) \simeq 1.0$ . Flux that doesn’t show up in these  $PC$  components must be redder yet to match the total ground-based (W91) and the global *HST* color of  $(B - I) \simeq 1.3$  (which is close to colors of the symmetric halo). If this feature is indeed a dust lane, it would have a differential optical depth between 1300 and 2400 Å ranging from  $\tau = 0.75 - 1.5$  averaged over the resolution limit. This is rather mild by standards of present-day galaxies. The visual or blue extinction expected for this amount of far-UV extinction would be easy to miss in nearby radio galaxies, so

the total amount of dust required is not excessive for objects like 53W002, which might be chemically younger and correspondingly more metal-poor.

## 4. Discussion and conclusions

### 4.1. Nature of the alignment effect in 53W002

The 8.4 GHz contours in Fig. 2 show that the radio source is *not* smaller than the distance between the blue continuum clouds, and that the radio jet coincides with the bright Ly $\alpha$  "arc" in the western cloud, suggesting that jet-induced star-formation could indeed cause both blue clouds, except the outer parts of the western cloud. The latter has a more "jagged, triangular" shape, as the color image of Plate 1 shows, and so may be caused by AGN light in reflection. A recent interferometric OVRO image of 53W002 in redshifted CO (J 3–2) — which has 3" FWHM — provides an important clue to the alignment effect (S97). The CO was detected up to 2–3" away on both sides of 53W002's AGN, *and in the same direction as both blue HST clouds and the extended 8.4 GHz radio source, but not perpendicular to this direction*, so that at least the CO that coincides with the currently visible jet was likely deposited there by physical processes related to this jet. Since Carbon and Oxygen had to be formed in massive stars, jet-induced star-formation thus likely played a role in 53W002. The CO extends further in both directions than the two aligned blue clouds and the current radio jet (Fig. 3 of S97 and Fig. 2a here). This is harder to understand through star-formation from the current compact jet, which is likely confined through a dense ISM in the galaxy (*cf.* de Vries et al. 1997), unless the jet in the past managed to get further out of the galaxy. This might be possible through holes in its dense ISM, if e.g. 53W002 formed through the rapid merging of surrounding sub-galactic sized objects (P96). 53W002's  $r^{1/4}$ -like stellar population is extended in the same direction as the radio source, so that the jet possibly triggered a non-negligible fraction of 53W002's

mass to form stars in these two directions. As long as this all happened within a few  $\times 10^8$  years, there could have been just enough time for the stellar population to settle into a possible  $r^{1/4}$ -like profile. Together with the continuum and  $\text{Ly}\alpha$  morphology of the blue clouds (§3.4 & Fig. 2), it thus appears that both reflection cones from an AGN (Fig. 1) and jet-induced star-formation are responsible for the alignment effect in 53W002.

We can compare the structure of 53W002 to the *HST* images of powerful radio galaxies of Longair, Best, & Röttgering (1995) and Best, Longair, & Röttgering (1996, 1997). From a set of eight 3CR radio galaxies at  $z \approx 1$ , they suggest that the morphologies change systematically with (projected) radio source size, and interpret this as evidence for jet-induced star formation in the aligned component. The radio galaxy 53W002 shares both properties with these powerful 3CR sources: a compact component — the AGN in the center of an extended starlight distribution — and a pair of clouds aligned with the projected radio axis. Contrary to the 3CR sources, we can already see a fairly relaxed symmetric distribution of starlight centered around 53W002’s nucleus. In hindsight, it is perhaps surprising to find the aligned component to be important even at these low radio powers, but the continuity of structure with the powerful radio galaxies is striking, and required the extra resolving power of the *WFPC2/PC* in the *B*-band to observe in detail.

#### 4.2. 53W002’s gas+dust content, surrounding cluster, and possible evolution

The measured  $\text{Ly}\alpha$  fluxes and broad-band UBVR<sub>I</sub>griJHK colors of 53W002 constrain its dust absorption ( $A_V \lesssim 0.2$  mag) and star formation rate (SFR; W91, W94b). Similar arguments have been made by P96 for the other 16 surrounding blue  $z = 2.40$  candidates. The SFR of 53W002 is of order  $\sim 100 M_\odot$  /year (W91), and  $\sim 5\text{--}10\times$  less for the other  $z = 2.40$  candidates (P96). The total stellar mass of 53W002 — integrated over its assumed exponentially declining SFR — is  $\sim 1.8 \times 10^{11} M_\odot$  (W91). The  $r^{1/4}$ -like light-profile of

53W002 suggests that at  $z = 2.39$  the object had already converted a non-negligible fraction of its gas mass into stars — rather efficiently on a  $\sim 0.4$  Gyr time-scale — suggesting a young early-type galaxy. The OVRO CO-flux of 1.5 Jy/km/s implies  $\sim 2.1 \times 10^{11} M_{\odot}$  in gas for 53W002 alone (S97). The velocity widths of the CO clouds are  $\sim 250$  km/s (HWHM), extending  $\sim 1''.5$  or  $\sim 13$  kpc on each side of 53W002 in the direction of the blue clouds *and* of the extended radio source, and possibly indicating a forming rotation curve (S97). These numbers imply an enclosed Keplerian mass of  $1.5\text{--}3.8 \times 10^{11} M_{\odot}$ , consistent with its total stellar mass above (W91). Taken together, this means that 53W002’s  $H_2(+CO)$  gas-mass could be  $\sim 30\text{--}60\%$  of its total (luminous+gas+dark) mass.

What could this mean for the evolution of 53W002? If all this gas settled into disk stars within a few free-fall times ( $\sim 1$  Gyr), 53W002 could evolve into an mid-type  $L^*$  spiral galaxy today (with  $B/D$ -ratio  $\sim 0.5$ ), or into an earlier-type galaxy ( $B/D \gtrsim 1$ ) if it did not, and if a substantial fraction remained neutral (as seen in some nearby ellipticals and merger remnants, *cf.* Hibbard 1995). The small velocity dispersion ( $\lesssim 300$  km/s) in P96’s group of  $z = 2.4$  objects with measured redshifts, and the small area ( $\lesssim 1$  Mpc<sup>2</sup>) over which the 16 surrounding sub-galactic objects are seen, suggests that many of these objects will likely merge into a few larger galaxies during the next half Hubble time after  $z \simeq 2.4$ . Hence, while 53W002 may have formed with a  $r^{1/4}$ -like profile during a relatively quick and sudden collapse that started at  $z \simeq 3$  ( $\sim 0.4$  Gyr before  $z = 2.4$ ) — possibly through star-formation along its radio jet — it also appears to be developing a massive disk at  $z \simeq 2.39$  (S97). This disk may have completely settled  $\sim 1\text{--}2$  Gyrs later (or at  $z \sim 1.5$ ), but possibly be destroyed again during future mergers (at  $z \lesssim 1.5$ ) with the surrounding sub-galactic sized objects (P96), so that the radio galaxy 53W002 may end up as a massive early-type galaxy today.

We thank Doug VanOrsow, Ray Lucas and the STScI staff for their assistance, Claudia Burg and Simon Driver for help in the image processing, Ed Fomalont for his recent VLA

positions, Jeff Hester, Dave Burstein and the referee for useful suggestions. This work was supported by NASA grants GO-5308.0\*-93A & GO-5985.0\*-94A (to both RAW and WCK) from STScI, which is operated by AURA, Inc., under NASA contract NAS5-26555.

## REFERENCES

- Best, P. N., Longair, M. S., & Röttgering, H. J. A. 1996, MNRAS, 280, P9
- Best, P. N., Longair, M. S., & Röttgering, H. J. A. 1997, MNRAS, 286, 785
- Chambers, K. C., Miley, G. K., & van Breugel, W. J. M. 1990, ApJ, 363, 21
- de Vries, W. H., et al. 1997, ApJS, 110, 191
- Driver, S. P., et al. 1995a, ApJL, 449, L23 (D95a)
- Driver, S. P., Windhorst, R. A., & Griffiths, R. E. 1995b, ApJ, 453, 48
- Eggen, O. J., Lynden-Bell, D., & Sandage, A. 1962 ApJ, 136, 748 (ELS62)
- Hibbard, J. 1995, Ph.D. thesis, Columbia University
- Longair, M. S., Best, P. N., & Röttgering, H. J. A. 1995, MNRAS, 275, P47
- Keel, W. C., & Windhorst, R. A. 1993, AJ, 106, 455
- McCarthy, P. J., van Breugel, W., Kapahi, V., & Subrahmanya, C. 1991, AJ, 102, 522
- Mutz, S., Windhorst, R., Wittman, D., Close, L., & McCarthy, D. 1997, AJ, 113, 1537
- Odewahn, S., Windhorst, R., Driver, S., & Keel, W. 1996, ApJL, 472, L013 (O96)
- Pascarelle, S., Windhorst, R., Keel, W., Odewahn, S. 1996b, Nature, 383, 45 (P96)
- Schmidtke, P. C., et al. 1997, AJ, 113, 569 (Sc97)
- Scoville, N., Yun, M., Windhorst, R., Keel, W., & Armus, L. 1997, ApJL, 485, L21 (S97)
- Searle, L. & Zinn, R. 1978, ApJ, 225, 357 (SZ78)
- van Albada, T. S. 1982, MNRAS, 201, 939

Windhorst, R. A., Franklin, B. E., Neuschaefer, L. W. 1994a, PASP, 107, 798

Windhorst, R. A., et al. 1994b, ApJ, 435, 577 (W94b)

Windhorst, R. A., Mathis, D. F., & Keel, W. C. 1992, ApJL, 400, L1 (W92)

Windhorst, R. A., et al. 1991, ApJ, 380, 362 (W91)

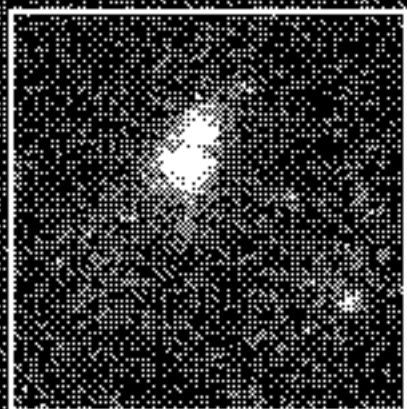
Windhorst, R. A., van Heerde, G. M., & Katgert, P. 1984a, A&AS, 58, 1 (W84a)

### Figure Captions

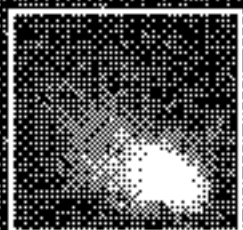
Fig. 1.— (COLOR PLATE 1). Color image of the *HST/PC* -exposures of the 53W002 field (12 hr in  $B_{450}$  & 5.7 hr in both  $V_{606}$  &  $I_{814}$  ). The  $V_{606}$  -band stack was rotated by  $6.721^\circ$  to match  $B_{450}$  &  $I_{814}$  (&  $\text{Ly}\alpha_{410}$  ), resulting in slanted borders, but small enough for all mosaics to cover roughly the same region (see D95a). North is  $140.3^\circ$  counterclockwise from vertical. This *PC* image covers  $32 \times 32''$  , and has  $\sim 0''.06$  resolution (FWHM). The  $3\text{-}\sigma$  point source sensitivity is 28.8 mag in  $B_{450}$  , 29.5 in  $V_{606}$  , 28.3 in  $I_{814}$  , and 26.6 mag in the 11.25 hr  $\text{Ly}\alpha_{410}$  images (Fig. 2a). The  $1\text{-}\sigma$  SB-sensitivity (per pixel) is  $26.7 \text{ mag arcsec}^{-2}$  in  $B_{450}$  , 26.8 in  $V_{606}$  , 26.2 in  $I_{814}$  , and 25.2 in  $\text{Ly}\alpha_{410}$  . The bright red object "S" is the only known star in the image. Other objects are labelled as in W91, W92, W94b, & P96. The inner light-profile of 53W002 is fairly regular, with a brighter blue "cloud" prominent to the upper-left ( $\simeq$ west; see Fig. 2). The WF2 inserts of the two  $z=2.40$  AGN (No. 18 & 19; P96) are shown at the same scale as the 53W002 insert, and show similar continuum cones.

Fig. 2.— (GLOSSY PLATE 2). Grey scale images of  $66 \times 66$  pixels ( $\simeq 3''.0 \times 3''.0$ ) of the *PC*-exposures on 53W002: (a)  $15 \times 2700\text{s}$  orbits in  $\text{Ly}\alpha_{410}$  ; (b)  $24 \times 2400\text{s}$  in  $B_{450}$  ; (c)  $12 \times 1700\text{s}$  in  $V_{606}$  ; (d)  $12 \times 1700\text{s}$  in  $I_{814}$  ; (e) equal to (b) after subtraction of a central point source (with 25% of the total  $B$ -band flux) and of the best fit  $r^{1/4}$ -like light-profile (Fig. 3 & §3.3); (f) the  $(B - I)$  color image as the ratio of (b)/(d). The VLA 8.4 GHz contours of W91 and the CO peaks of S97 are superimposed in (a) & (d) (see text). The AGN is located at each panel's central pixel. *Note:* the low SB and "arclike" feature of the  $\text{Ly}\alpha$  cloud in (a); the  $r^{1/4}$ -like bulge and brighter blue cloud in (b)–(d); the brighter *and* fainter blue clouds in (e) where the symmetric parts of 53W002 have been subtracted; and the blue (dark) central AGN and the small reddish (white) linear feature separating both blue clouds in (f). The radio source covers most of the blue clouds plus the  $\text{Ly}\alpha$  "arc", suggesting jet-induced starformation; the remainder of the continuum and  $\text{Ly}\alpha$  cloud may be reflected AGN light.

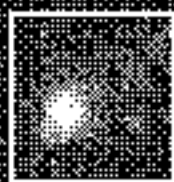
Fig. 3.— SB profiles in  $B_{450}$ ,  $V_{606}$  &  $I_{814}$  vs. radius (in  $r^{1/4}$  units) for the extended component of the radio galaxy 53W002 at  $z = 2.390$  in the quadrant that is relatively free of the blue clouds. The  $V_{606}$  profile was moved up by  $-0^m2$  for clarity. A central AGN component was subtracted in each filter, using star "S" as PSF (Fig. 1). Short dashes represent the 25% AGN component in  $B$ , which affects the profile to the left of the vertical dashed line ( $r^{1/4} \lesssim 0.5$ ;  $r \lesssim 0''.06$ ). Formal errors reflect photon statistics only. Horizontal dotted lines indicate  $2\sigma$  sky-subtraction errors, which affect the profiles for  $r^{1/4} \gtrsim 0.75$ – $0.8$  ( $r \gtrsim 0''.4$ ). For  $0.5 \lesssim r^{1/4} \lesssim 0.75$  ( $0''.06 \lesssim r \lesssim 0''.4$ ), 53W002's profile is consistent with an  $r^{1/4}$ -law, especially if the AGN contribution is  $\leq 20\%$ , but at large radii it is affected by the blue clouds.



Obj. 18



53W001



Obj. 19

Obj. 5

53W002

5

6

7

